An Analysis of Sliding Mode Speed Controller for a Differential Drive Wheel Mobile Robot

Tri-Vien VU[1,*], *Anh-Minh Duc TRAN*[2]

[1]Modeling Evolutionary Algorithms Simulation and Artificial Intelligence, Faculty of Electrical and Electronics Engineering, Ton Duc Thang University, Ho Chi Minh City, Vietnam.
[2]Faculty of Electrical and Electronics Engineering, Ton Duc Thang University, Ho Chi Minh City, Vietnam.

*Corresponding Author: Tri-Vien Vu (Email: vutrivien@tdtu.edu.vn)
(Received: 10-December-2023; accepted: 14-March-2024; published: 31-March-2024)
http://dx.doi.org/10.55579/jaec.202481.445

Abstract. *In this study, we present a systematically designed Sliding Mode Speed Controller (SMSC) tailored for motors utilized in a Differential Drive Wheel Mobile Robot (DDWMR). Our analysis delves into the critical parameters of the SMSC, including convergence and reaching rates, alongside simulation configurations such as time step. We concurrently consider metrics like rising time, steady-state error, and control ripple factors to optimize performance. Through comprehensive evaluation across various case studies, we demonstrate the efficacy of the fine-tuned SMSC in enhancing the overall performance of the DDWMR. Our simulation results underscore the significance of meticulous parameter tuning, particularly emphasizing the role of time step settings. We find that a smaller time step mitigates chattering phenomena and improves performance, albeit at the cost of increased computational demands and potentially heightened hardware requirements.*

Keywords: SMC, Control-oriented, differential drive, Wheel mobile robot, Speed controller

1. Introduction

One of the most common types of mobile robots is wheel mobile robots (WMRs). This type of robot utilizes wheels for locomotion. Due to their simplicity, affordability, and versatility, WMRs are used in a wide variety of applications. This kind of robot can be utilized for medications and supplies delivery in hospitals and other healthcare facilities [1, 2]. For manufacturing and logistics, WMRs can be used to deliver goods and material handling in indoor, urban and suburban areas [3–5]. Path guiding and customer servicing are common tasks that WMRs can also be utilized in the retail and services domains [6, 7]. In the field of education, mobile robots are widely used as learning and research tools in universities and research institutions worldwide. They play a crucial role in equipping students, scholars, and researchers in the fields of robotics and artificial intelligence with knowledge and skills [8–10]. Lots of applications of WMRs can be found in other fields such as security, agriculture, and space exploration.

In mobile robots, each robot typically has several driving wheels that are actuated by electrical motors. Most of published works used per-

manent magnet direct current (PMDC), brushless direct current (BLDC), step, or dc servo motors. The motors were considered as either torque sources, which serve as inputs to the dynamic model, or speed sources for the kinematic model of the robots. This means that the control system is designed to control the motors in order to track a desired trajectory, either by regulating the torque or speed of the motors. However, no detail speed control system design for the motors was discussed in the mentioned works.

For dc motors, the interested control problems are typically speed, torque, and/or position control. These problems can be solved by utilizing various linear and nonlinear control techniques, such as PI/PID [11–15], pole-placement for MIMO system [16], active damping injection [17], soft computing technique [18, 19], adaptive controller [20, 21], model predictive control [22–25]. In all these mentioned works, DC motors were considered standalone systems, with a constant, a step change, or some bounded noise load torques. Practically, the performance of these controllers can differ greatly when applied to standalone DC motors versus DC motors used in mobile robots. In addition, several parameters of the mobile robots are not exactly known and/or not to be constants during operation. In this case, robust control techniques should be used.

Built on the theory of variable structure control, sliding mode control (SMC) method is a robust nonlinear control technique [26]. The SMC can be applied to a variety of electrical drives systems, including direct current drives [27, 28], induction motor drives [29], permanent magnet synchronous motor drives [30–32], or piezoelectric actuator [33]. For mobile robots, SMC are mostly used for trajectory tracking [34–37], in which the SMC enables the mobile robot to achieve better trajectory tracking in the presence of external disturbance and un-modelled dynamics. In all SMC-related mentioned works, the parameters of the SMC were designed and selected intuitively. No discussion has been made about the effects of the parameters or how to obtain suitable values. In addition, the effect of simulation time step has not been addressed in the published works.

In this work, considering longitudinal dynamic of a wheel mobile robot only, a control-oriented model is derived and used for designing a SMSC for the DC motor. The effect of the multi-motor coupling characteristics and unmodelled dynamics are considered lumped and bounded disturbance terms.

The investigation will delve into the effects of SMSC parameters, including convergence and reaching rates, alongside simulation configurations, such as the time step. We will simultaneously consider metrics like rising time, steady-state error, and control ripple factors to meticulously select optimal values for both controller parameters and simulation settings.

We will assess the performance of the sliding mode speed controller with optimized parameters across the entirety of the DDWMR system. Relative Root Mean Square Error (RRMSE) metrics are defined and will serve as the benchmark for evaluating the tracking performance of individual left and right motors, as well as the overall robot dynamics.

The remainder of this work is organized as follows. Section II introduces the development of the control-oriented model and outlines the systematic approach employed in designing the sliding mode speed controller. Section III elaborates on the performance evaluation of the designed controllers, both in standalone motor systems and within the complete DDWMR system. Finally, Section IV highlights the main contributions of this study and outlines potential directions for future research endeavors.

2. Sliding mode speed controllers

2.1. Longitudinal control oriented model

The DDWMR in this work actuated by two permanent magnet direct current motors which are connected to the corresponding left- and right-wheel through gearboxes as shown in Fig 1 below. Two caster wheels are located at front and rear for balancing. The center-of-mass is as-

sumed located at the center of geometry. In order to design the speed controller for the PMDC motors in the DDWMR, a simplified half-weight model of the DDWMR is proposed. In this model, the DDWMR is assumed symmetrically along its x-axis, when only considering the longitudinal dynamic, the force diagram of the system is depicted as in 2. In this work, the proposed robot is assumed working on a planar surface. Since the robot velocity is relative low, aerodynamic drag force can be neglecting. The simplified longitudinal dynamic equation of a half-weight mobile robot can be obtained as [43]:

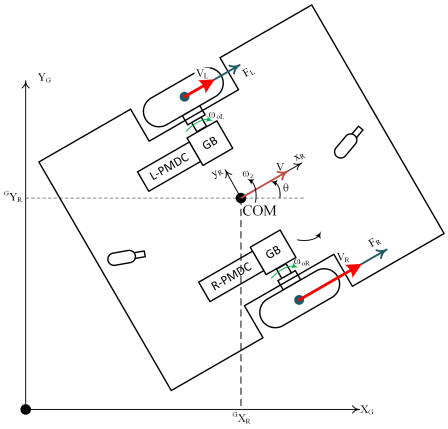

Fig. 1: DDWMR diagram.

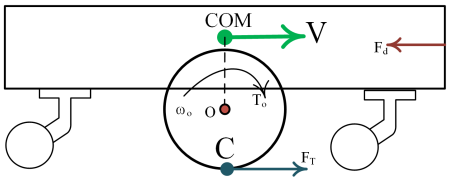

Fig. 2: Longitudinal dynamic diagram.

$$F_T - F_d = \frac{m}{2}\frac{dV}{dt} \tag{1}$$

where F_T is the traction force generated by the driving wheel at the ground contact point C, F_d is the lumped disturbance force due to the coupling effect between the two driving wheels and the frictional forces at the caster wheels, m is the total weight of the robot, V is the longitudinal velocity of the robot.

The traction force is depended on the friction between the wheel and the ground. For most indoor mobile robots, the wheel is rolled without slipping, the traction force is only depended on the moment of inertia of the wheel as

$$T_o - F_T R_w = J_w \frac{d\omega_o}{dt} \tag{2}$$

where T_o, ω_o are the torque and angular speed at the output shaft of the gearbox, R_w is the wheel radius, J_w is the wheel moment of inertia. The relationship between the robot velocity and the wheel angular speed is

$$V = R_w \omega_o \tag{3}$$

When the gearbox has speed ratio of i_G and transmission efficiency of η_G, the relationship between the input and output of the gearbox is expressed by

$$\begin{aligned} T_i &= \frac{1}{i_G \eta_G} T_o \\ \omega_m &= i_G \omega_o \end{aligned} \tag{4}$$

Where T_i is the torque at the input shaft of the gearbox and ω_m is the angular speed of the PMDC motor whose dynamic expressed by

$$\begin{aligned} \frac{di_a}{dt} &= -\frac{R_a}{L_a} i_a - \frac{K_E}{L_a}\omega_m + \frac{1}{L_a} U_a \\ T_m - T_i - B_m \omega_m &= J_m \frac{d\omega_m}{dt} \end{aligned} \tag{5}$$

Where i_a is the current, R_a is the resistance, L_a is the inductance, U_a is the voltage of the armature winding; is the torque, K_T is the torque constant, K_E is the voltage constant, B_m is the viscous coefficient, J_m is the moment of inertia of the PMDC motor.

After some mathematical manipulation, above equations can be rearranged in terms of the armature current and angular speed of the PMDC as:

$$\begin{aligned} \frac{di_a}{dt} &= -\frac{R_a}{L_a} i_a - \frac{K_E}{L_a}\omega_m + \frac{1}{L_a} U_a \\ \frac{d\omega_m}{dt} &= \frac{K_T}{J_T} i_a - \frac{B_m}{J_T}\omega_m - \frac{R_w}{\eta_G i_G J_T} F_d \end{aligned} \tag{6}$$

where $J_T = J_m + \frac{J_w}{\eta_G i_G^2} + \frac{m R_w^2}{2\eta_G i_G^2}$ is the total moment of inertia of the half-weight robot and $T_d = \frac{R_w}{i_G \eta_G} F_d$ is the disturbance torque referred to the motor shaft. After eliminating the armature current and its derivative in equation 6,

the dynamic of the robot can be referred to the PMDC motor's dynamics as:

$$\ddot{\omega}_m = -a_1\dot{\omega}_m - a_2\omega_m + a_3U_a - a_4\dot{T}_d - a_5T_d \quad (7)$$

where

$$a_1 = \frac{R_a}{L_a} + \frac{B_m}{J_T}; a_2 = \frac{R_aB_m}{L_aJ_T} + \frac{K_EK_T}{L_aJ_T};$$
$$a_3 = \frac{K_T}{L_aJ_T}; a_4 = \frac{1}{J_T}; a_5 = \frac{R_a}{L_aJ_T}$$

2.2. Sliding mode speed controller (SMSC)

When using the rolling without slipping assumption, the robot velocity is proportional to the motor angular speed. It is obviously that a better motor speed tracking resulting in a better robot tracking accuracy. Hence, in this work, we propose a SMSC for PMDC motors in order to improve the trajectory tracking capability of the DDWMR.

The speed error is defined as the different between the desired speed and the actual speed measured from encoder.

$$e = \omega_{m,ref} - \omega_m \quad (8)$$

Let $x_1 = \omega_{m,ref} - \omega_m; x_2 = \dot{\omega}_{m,ref} - \dot{\omega}_m$, the equations of error dynamic become:

$$\dot{x}_1 = x_2$$
$$\dot{x}_2 = \begin{pmatrix} \ddot{\omega}_{m,ref} + a_2\left(\omega_{m,ref} - x_1\right) \\ +a_1\left(\dot{\omega}_{m,ref} - x_2\right) - a_3U_a + f\left(t\right) \end{pmatrix} \quad (9)$$

where $f(t)$ is the time function depended on disturbances as

$$f\left(t\right) = a_4\dot{T}_d + a_5T_d \quad (10)$$

The switching function of the SMC is defined as

$$s = x_2 + \lambda x_1 \quad (11)$$

where λ is a constant determining the rate of convergence of the switching phase. Take the first derivative of equation (11) we obtained:

$$\dot{s} = \dot{x}_2 + \lambda\dot{x}_1 \quad (12)$$

Substitute equation 9 into 12 we have:

$$\dot{s} = \begin{pmatrix} \ddot{\omega}_{m,ref} + a_2\omega_{m,ref} + a_1\dot{\omega}_{m,ref} \\ -a_1x_2 - a_2x_1 - a_3U_a + f\left(t\right) + \lambda x_2 \end{pmatrix} \quad (13)$$

and

$$s\dot{s} = s\begin{pmatrix} \ddot{\omega}_{m,ref} + a_2\omega_{m,ref} + a_1\dot{\omega}_{m,ref} \\ -a_1x_2 - a_2x_1 - a_3U_a + f\left(t\right) + \lambda x_2 \end{pmatrix}$$

Select a Lyapunov candidate function as

$$V = \frac{1}{2}s^2 \quad (14)$$

It is obviously that V is satisfied the first three properties of a Lyapunov function. The switching system will be asymptotically stable if:

$$\dot{V} = s\dot{s} \leq 0 \quad (15)$$

The reaching law is defined as

$$\dot{s} = -qsign\left(s\right) \quad (16)$$

where $q > 0$ is the constant rate and the sign function is defined as

$$sign\left(s\right) = \begin{cases} 1 & s > 0 \\ 0 & s = 0 \\ -1 & s < 0 \end{cases} \quad (17)$$

Then

$$s\dot{s} = \begin{cases} -qs < 0 & \text{when } s > 0, q > 0 \\ 0 & \text{when } s = 0 \\ qs < 0 & \text{when } s < 0, q > 0 \end{cases} \quad (18)$$

Hence, equation 15 is satisfied with all value of s. Equaling 13 and 16 we have

$$u = \frac{1}{a_3}\left[\begin{array}{l} \ddot{\omega}_{m,ref} + a_1\dot{\omega}_{m,ref} + a_2\omega_{m,ref} \\ -a_2x_1 - a_1x_2 + \lambda x_2 + qsign\left(s\right) + f\left(t\right) \end{array}\right] \quad (19)$$

where u is the desired armature voltage.

It can be seen that the control law from 19 is completed if the disturbance $f(t)$ is known which is impractical. However, it is reasonable to assume that the disturbance and its rate of change are bounded, that are:

$$\begin{aligned} T_{dL}\left(\mathbf{x},t\right) \leq T_d \leq T_{dU}\left(\mathbf{x},t\right) \\ \dot{T}_{dL}\left(\mathbf{x},t\right) \leq \dot{T}_d \leq \dot{T}_{dU}\left(\mathbf{x},t\right) \end{aligned} \quad (20)$$

where the bounds T_{dL}, T_{dU}, $\dot{T}_{dL}$, and $\dot{T}_{dU}$ are known. In this case, the disturbance and its rate

of change in $f(t)$ of 19 is replaced by corresponding conservative quantities T_{dc} and $\dot{T}_{dc}$.

$$u = \frac{1}{a_3}\begin{bmatrix} \ddot{\omega}_{m,ref} + a_1\dot{\omega}_{m,ref} + a_2\omega_{m,ref} \\ -a_2x_1 - a_1x_2 + \lambda x_2 \\ -qsign\,(s) + a_4\dot{T}_{dc} + a_5T_{dc} \end{bmatrix} \tag{21}$$

Substitute equation 21 into 13 and simplifying the results, we obtained:

$$\dot{s} = -qsign\,(s) + a_4\left(\dot{T}_d - \dot{T}_{dc}\right) + a_5\left(T_d - T_{dc}\right) \tag{22}$$

As has been proved in previous section, the term $-sqsign\,(s)$ is negative with all value of s.

Hence to ensure $s\dot{s} \leq 0$, the conservative quantities are selected as:

$$\begin{aligned} if\, s \geq 0 \quad select &\begin{cases} \dot{T}_{dc} = \dot{T}_{dU} \geq \dot{T}_d \\ T_{dc} = T_{dU} \geq T_d \end{cases} \\ if\, s < 0 \quad select &\begin{cases} \dot{T}_{dc} = \dot{T}_{dL} \leq \dot{T}_d \\ T_{dc} = T_{dL} \leq T_d \end{cases} \end{aligned} \tag{23}$$

Let

$$\begin{aligned} d\bar{T}_{1d} &= \frac{\dot{T}_{dU} - \dot{T}_{dL}}{2}; d\bar{T}_{2d} = \frac{\dot{T}_{dU} + \dot{T}_{dL}}{2} \\ \bar{T}_{1d} &= \frac{T_{dU} - T_{dL}}{2}; \bar{T}_{2d} = \frac{T_{dU} + T_{dL}}{2} \end{aligned} \tag{24}$$

Then we have

$$\begin{aligned} dT_{dc} = \dot{T}_{dc} &= d\bar{T}_{2d} - d\bar{T}_{1d}sign\,(s) \\ T_{dc} &= \bar{T}_{2d} - \bar{T}_{1d}sign\,(s) \end{aligned} \tag{25}$$

The control law is finally as

$$u = \tfrac{1}{a_3}\begin{bmatrix} \ddot{\omega}_{m,ref} + \lambda\dot{\omega}_{m,ref} + (a_1 - \lambda)\,\dot{\omega}_m + a_2\omega_m \\ +qsign\,(s) \\ +a_4dT_{dc} + a_5T_{dc} \end{bmatrix} \tag{26}$$

For easy understanding, the control law is decomposed into three components as:

$$u = u_{eq} + u_{sw} + u_{dr} \tag{27}$$

in which

$$u_{eq} = \frac{\ddot{\omega}_{m,ref} + \lambda\dot{\omega}_{m,ref} + (a_1 - \lambda)\,\dot{\omega}_m + a_2\omega_m}{a_3} \tag{28}$$

$$u_{sw} = \frac{qsign\,(s)}{a_3} \tag{29}$$

$$u_{dr} = \frac{a_4}{a_3}dT_{dc} + \frac{a_5}{a_3}T_{dc} \tag{30}$$

where u_{eq} is the equivalent control which drives the system sliding on the sliding surface, $\dot{s} = 0$, under ideal situation where all information of the system is known and no disturbance; u_{sw} is the switching component which drives the system to the sliding manifold and u_{dr} is disturbance rejection term. The disturbance rejection component is added to the system in the reaching phase to eliminate the effect of disturbance of the system such as load torque variation.

3. Simulation results and discussion

In this section, several case studies will be implemented and investigated. Initially, the effect of the simulation time step will be investigated. After that, with a reasonable time step, the effect of the reaching rate and convergence rate of the SMSC will be evaluated. Considering rising time, steady state error, and control signal fluctuation, the suitable value of reaching rate and convergence rate of the SMSC will be selected. Then these SMSCs will be applied to the PMDC motors used in the proposed DDWMR to investigate the performance of the whole system.

The sliding mode speed controller for PMDC motor is built in Matlab/Simulink as shown in Fig 3a below. The SMC, Eq. 27, is built as Matlab function blocks as shown in Fig. 3b In order to evaluate the disturbance rejection capability of SMSC, two SMSCs are built, one is without disturbance rejection component, $u_{dr} = 0$, and one with disturbance rejection component. This component is integrated into the same block by adding the term d into Eq. 30, $d = 0$ is woTd-SMC, and $d = 1$ is for wTd-SMC.

$$u_{dr} = d\left(\frac{a_4}{a_3}dT_{dc} + \frac{a_5}{a_3}T_{dc}\right) \tag{31}$$

The parameters used for simulation are listed in Table 1.

3.1. Case Study (CS) 1: Time step effects

In this case study, the time step is set as 1e-6s as shown in Fig. 4. The disturbance is assumed

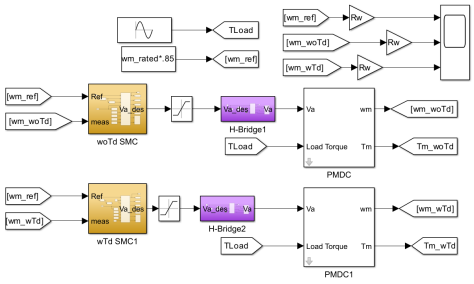

(a) System block diagram

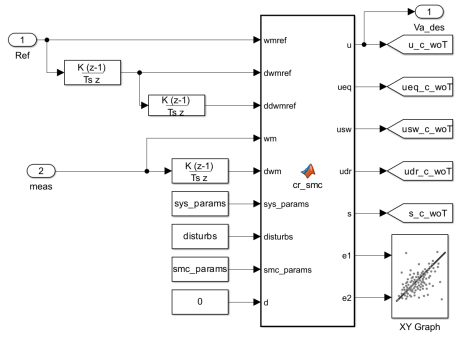

(b) SMC without disturbance rejection

Fig. 3: Simulation model.

Tab. 1: System parameters

No.	Parameter [Unit]	Description	Value
1	Va [V]	Rated Voltage	48
2	P_n [W]	Rated Power	350
3	N_n [rpm]	Rated Speed	560
4	R_a [Ω]	Armature Resistance	0.93
5	L_a [mH]	Armature Inductance	150
6	J_m [$Kg.cm^2$]	Moment of Inertia	15
7	B_m [N.cm/rad]	Viscous Coefficient	1.1
8	K_T [N.m/A]	Torque Constant	0.58
9	K_E [V/rad]	Voltage Constant	0.58

the frictional forces. The controller parameters are arbitrary set as $q = 1.8$; $\lambda = 0.01$. The configuration parameters for simulation in this case study are set as shown in Fig. 4.

The results of CS1 are shown in Fig.5. If considering the performance of the system output only as shown in Fig. 5a, it seems that the system has perfectly performance. There is no different between with and without disturbance rejection, no steady state error, very short rising time, no overshoot, etc. Fig. 5b showed that the value of load torque is insignificant in comparing with the motor torque, hence the effect of the load toque is ignorable. However, when considering each component of the controller output shown in Fig. 5c, it can be seen that the equivalent component has a very high value, more than $2e^{10}$. When the equivalent component is relative high, the effect of others is insignificant. That why the value of the SMSC parameters, λ and q, can be selected arbitrary small. The observed phenomenon occurs because of the small time step setting. Since the simulation time step is $1e^{-6}$, the extremely higher rate of change of reference speed and acceleration will be obtained causing a relative high value of equivalent component of the SMSC due to Eq. 28. For practical

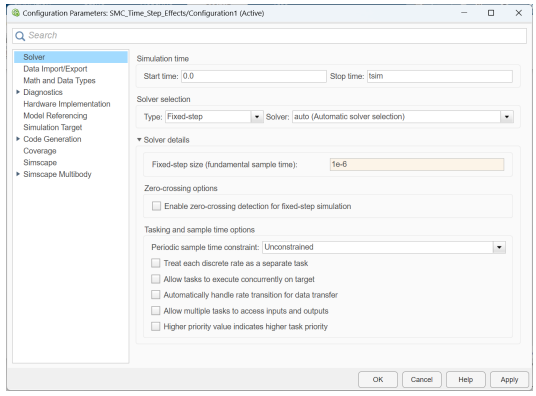

Fig. 4: Simulation configuration.

systems, the simulation time step should be selected more reasonable. Hence, in the next step, the simulation is conducted with different value of time step. The results are shown in Fig. 6. It can be seen that the system fails when the time step is larger than 0.01s with SMC has $q = 1.8$ and $\lambda = 0.01$

3.2. CS2: Reaching rate effect

In this case study, the effect of the reaching rate constant is investigated. In this case, the step time is 0.01s, $\lambda = a_1$. The value of q is randomly selected as $[0.5a_3 1.5a_3 2.5a_3 15a_3]$. The robot is forced to track a step reference speed. The effect of q on the output of the system is shown in Fig. 7 below. It can be seen that if the value of q is not large enough, the system cannot track the reference speed. In addition, when the value of q is increased, the effect of the disturbance

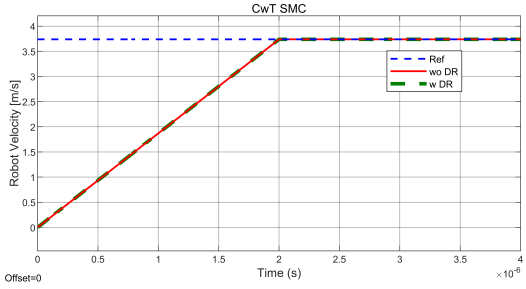

(a) Robot velocity

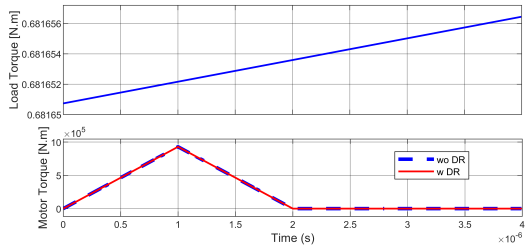

(b) Motor torque and load torque

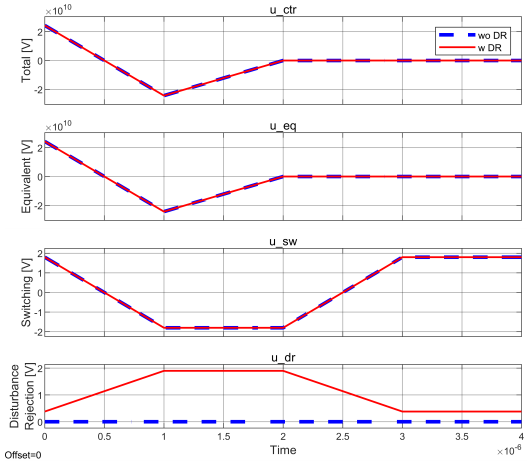

(c) Control signal components

Fig. 5: Simulation results for CS1.

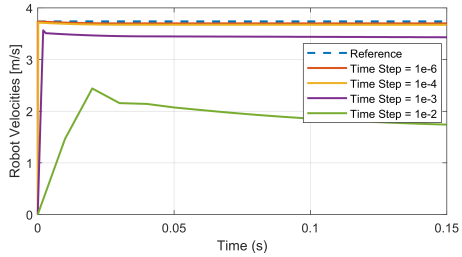

Fig. 6: Time step effects.

rejection component will be reduced. For high enough value of q, there is insignificant different between the system performance under without and with disturbance rejection. On the other words, with the suitable value of q, the conventional SMSC still be able to reject the disturbance. Thereafter the SMC without disturbance rejection will be used in this work.

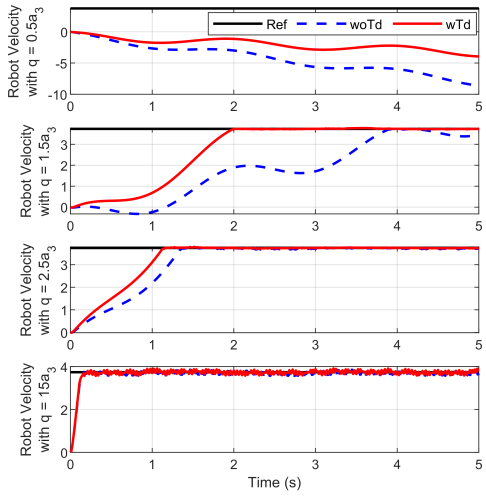

Fig. 7: Reaching rate effect on the output.

3.3. CS3: Optimum reaching rate value

In order to find the optimum value of q, it is necessary to consider both the rising time and the tracking performance. The rising time is the period that the system requires to reach 95% its speed reference from standstill condition. The tracking performance is evaluated by using the

relative root-mean-square error defined as

$$\mathrm{RRMSE}\,(\%) = \frac{\sqrt{\frac{1}{\mathrm{n}}\sum_{\mathrm{i}=1}^{\mathrm{n}}\left(\mathrm{y_{ref}} - \mathrm{y_m}\,(\mathrm{i})\right)^2}}{\mathrm{y_{ref}}} \times 100 \tag{32}$$

where n is the number of simulation steps, y_{ref} is the reference and y_m is the measured angular speed of the motor.

In this case study, the value of q is spanning from $3a_3$ to $100a_3$. The effect of q on the RRMSE and the rising time are shown in Fig. 8. As has been seen in Fig. 5, higher value of q makes smaller RRMSE and shorter rising time. However, when increasing q, the value of switching component also increased. As a consequence, the output is fluctuated. In contrast, the rising time is tended to converge. Considering both the RRMSE and the rising time, the optimal reaching rate can be found as $q = 8735 (= 42.62a_3)$ with the corresponding rising time $tr = 0.08$sec and RRMSE $= 11.5\%$. When considering the

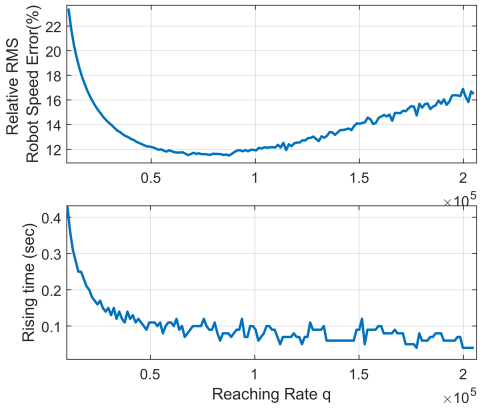

Fig. 8: Reaching rate effects.

last 500 data points, the steady state RRMSE is as shown in Fig. 9. It can be seen that if the value of q is not large enough, the system cannot reach its reference value. The system achieves smallest steady state RRMSE of 2.84% with$q = 18954$ (equal to $9.54a_3$). The higher value of q causes a higher steady fluctuation amplitude, hence a larger RRMSE. Fig. 10 below illustrates the effects of q on the performance of the system under three situations: overall optimal RRMSE, steady state optimal RRMSE, and very large reaching rate, $q = 100a_3$.

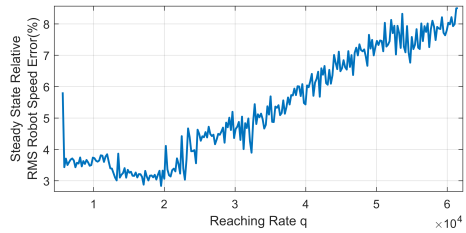

Fig. 9: Rate reaching effects on steady State RRMSE.

3.4. CS4: Reaching rate and convergence rate effects

In this case study, the performance of the system is evaluated under different values of reaching rate and convergence rate. The value of reaching rate is swept from $1.75a_3$ to $50a_3$ while the value of the convergence rate is swept from $0.5a_1$ to $3a_1$. In order to evaluate the chattering of the control signal, the ripple factor of the control signal is used. The ripple factor is defined by equation below. This factor is originally used to evaluate the quality of a rectifier, whose converts alternative current into direct current.

$$C_{rf} = \sqrt{\left(\frac{u_{rms}}{u_{avg}}\right)^2 - 1} \tag{33}$$

where $u_{rms}$is the root mean square value and u_{avg} is the average value of the control signal. The simulation results are shown in Fig. 11 below. The optimal value for the reaching rate is $q = 30a_3$ and for the convergence rate is $\lambda = 0.75 * a_1$.

3.5. CS5: Effect of SMSC on the DDWMR

Finally, the performance of the proposed controller is evaluated when applying for the whole DDWMR. The block diagram of the system is shown in Fig. 12. Details about modeling and simulation of the DDWMR can be found in our previous work [16]. In this case study, the left and right motor-wheel are assumed different. Their parameters are listed in Table 2.

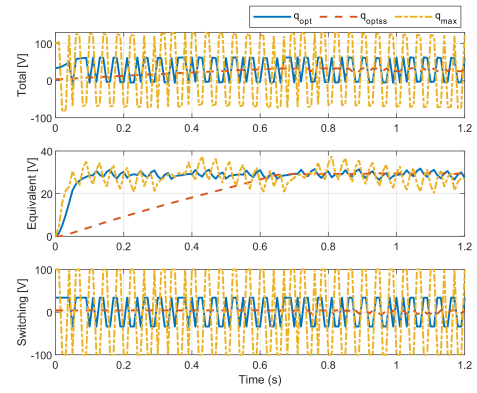

(a) Control components

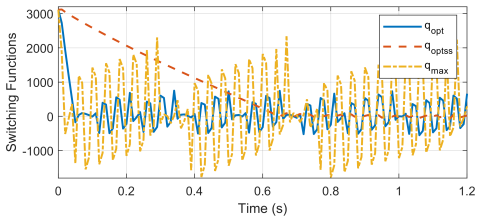

(b) Switching function

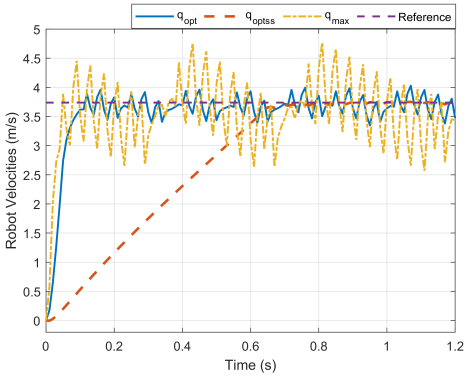

(c) Reference tracking

Fig. 10: Typical reaching rate values.

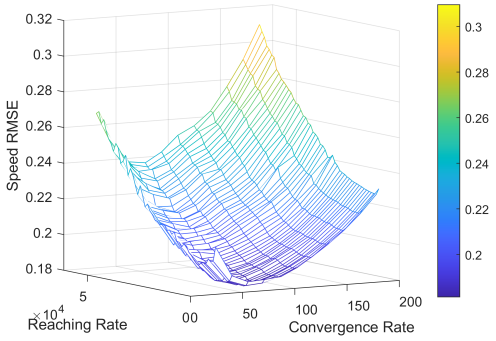

(a) Effect of convergence and reaching rates

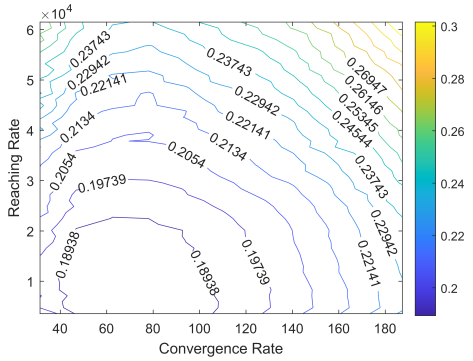

(b) Contour of the RRMS Errors

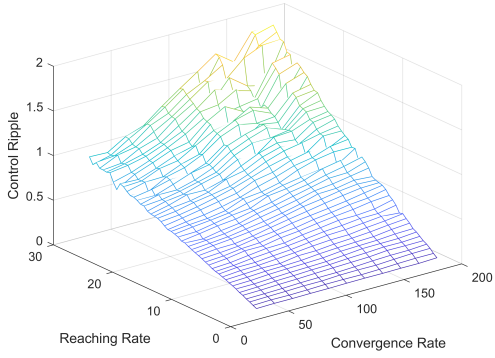

(c) Control ripple

Fig. 11: Reaching and convergence rates effects.

This approach makes the model of the proposed DDWMR more general [39]. Other parameters are as listed in Table 1.

In this case study, the linear and angular velocities of the robot are forced to track desired values which are given in term of trapezoidal velocity profiles. The robot is commanded to move forward and backward, respectively. During the forward the robot is commanded to turn left and then turn right. Also during the backward movement, the robot is commanded to turn right and then turn left. For simulation, the time-step settings is$5e^{-3}$. The load torque disturbance assumed a band-limited width noise as shown in Fig.13. From the desired linear and angular velocities of the robot, the inverse kinematic model of DDWMR is utilized to estimate the reference

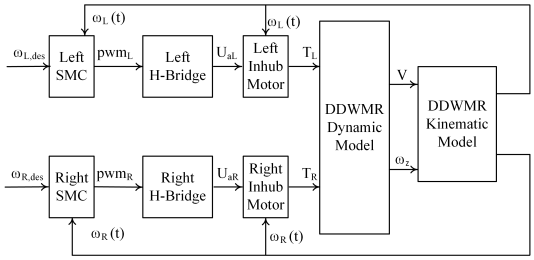

Fig. 12: Block diagram of the DDWMR.

Tab. 2: System parameters for a general DDWMR

No.	Parameter [Unit]	Description	Value	
			PMDC Motors	
			Left	Right
1	R_a [Ω]	Armature Resistance	1.12	0.74
2	L_a [mH]	Armature Inductance	127	172
3	J_m [$Kg.cm^2$]	Moment of Inertia	17	14
4	B_m [N.cm/rad]	Viscous Coefficient	0.88	1.32
5	K_T [N.m/A]	Torque Constant	0.52	0.63
6	K_E [V/rad]	Voltage Constant	0.52	0.63
7	m_w [Kg]	Motor-wheel Weight	3.45	2.55

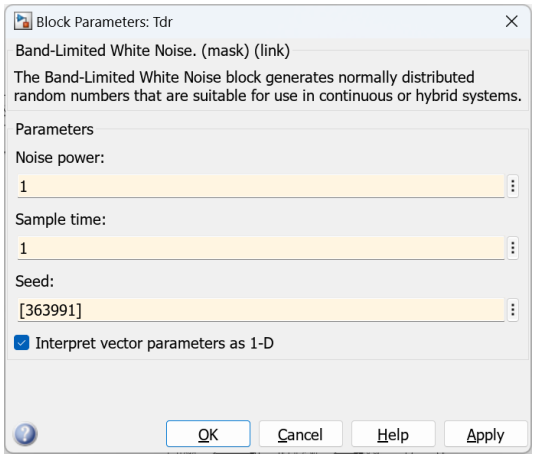

Fig. 13: Load torque disturbances setting.

left and right motor angular speed.

$$\omega_{mR,des} = \frac{V_{des} + W\omega_{z,des}}{R_{wR}}$$
$$\omega_{mL,des} = \frac{V_{des} - W\omega_{z,des}}{R_{wR}} \quad (34)$$

The errors between the desired value and the measured value of the motor angular speeds will be fed into the SMSCs. The output of the SMSCs are the pulse-width-modulation signals that will be provided to the H-bridges. The outputs of the H-bridges are the armature voltages applying to the PMDC motors.

To evaluate the performance of the system under different speed controllers, the relative root-mean-square error in Eq. 32 is modified as

$$\mathrm{RRMSE}\,(\%) = \frac{\sqrt{\sum_{i=1}^{n} \left(y_{ref}\,(i) - y_m\,(i)\right)^2}}{\sqrt{\sum_{i=1}^{n} y_{ref}^2\,(i)}} \times 100 \quad (35)$$

where n is the total simulation steps.

The responses of the motors and the robot velocities are shown in Fig.14. It can be seen that the motors track their references in a reasonable manner. If only considering Fig. 15a, it seems that the outputs are nearly identical to the reference. However, there are errors as shown in Fig. 15b. The RRMSE(%) of the left and the right motor are 2.59% and 2.57%, respectively. The linear velocity tracking error is smallest, only about 1%. The angular speed tracking error is relatively large, 16.71% and with a high frequency fluctuation. The reason is even the motors are tracking to their reference but the response time and the occurrence of disturbance of each motor is different. The overview of the

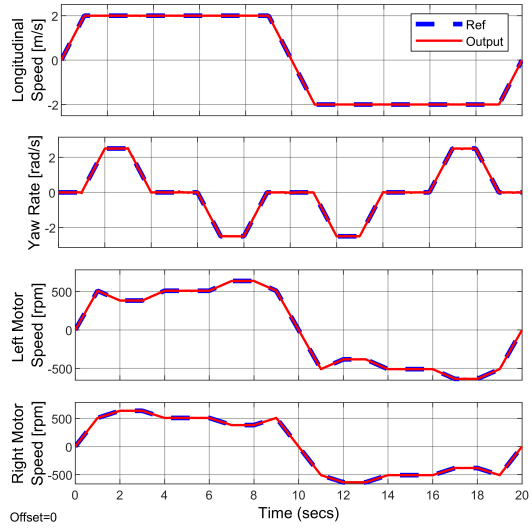

Fig. 14: Velocity responses.

load torques, and the output torques of the right and the left motors are shown in Fig. 15a and the details are shown in Fig. 15b. It can be seen that the motor torques are fluctuated with high

frequency. This phenomenon is chattering problem of conventional sliding mode control technique when the time step is relative large.

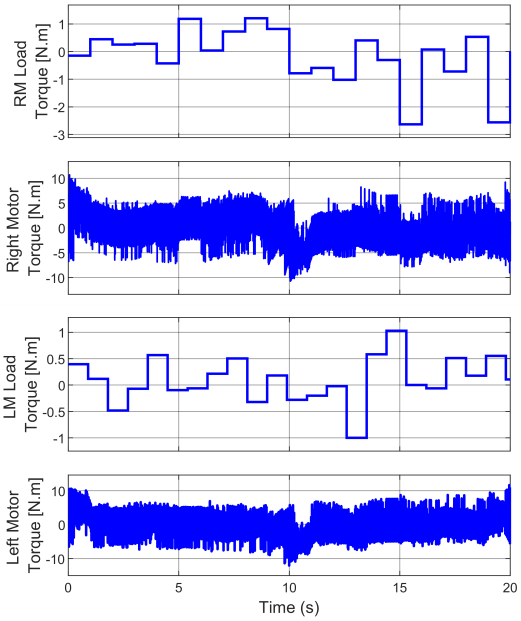

(a) Overall

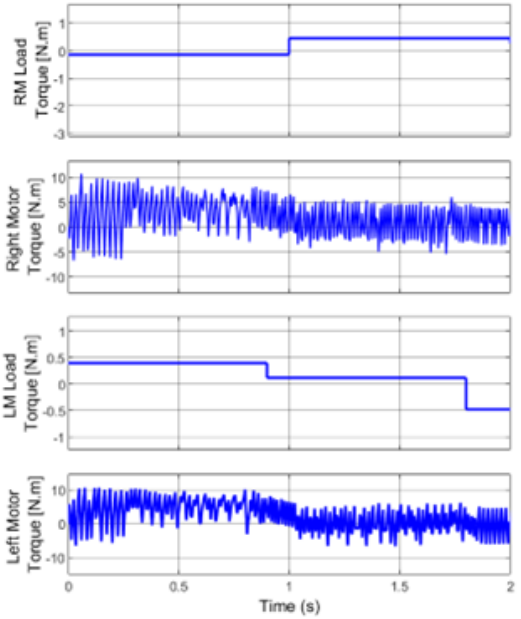

(b) Detail

Fig. 15: Load torques and motor torques.

Similar simulations have been taken placed with a smaller time step setting, $1e^{-4}$. The RMSE and RRMSE of motor response and the DDWMR responses are summarized up in Table 3. The errors of the motor and the robot velocities with two time-step settings are shown in Fig. 16. When the time step is $1e^{-4}$, the outputs are nearly identical to the corresponding references. For simulation, the smaller time step means the higher computational time consumption. For practical system, smaller time step requires stronger hardware capability. It is recommended that suitable time step setting should be considered for particular systems and applications.

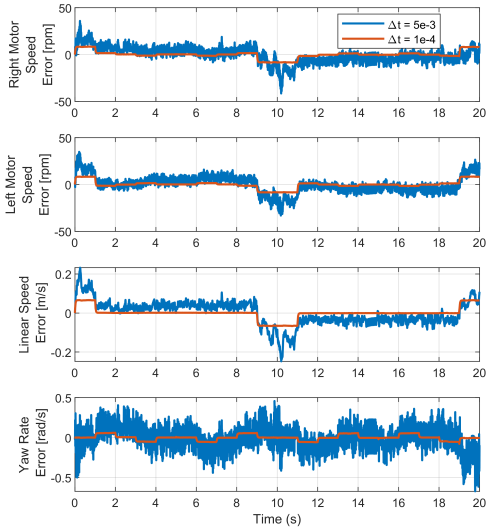

Fig. 16: Velocity errors with different time step settings.

Tab. 3: Time step effects

No.	Time Step	Metrics	Right Motor [rpm]	Left Motor [rpm]	Linear Speed [m/s]	Yaw Rate [rad/s]
1	$5e^{-3}$	RMSE	9.26	9.18	0.054	0.24
		RRMSE	2.59	2.57	0.93	16.73
2	$1e^{-4}$	RMSE	3.76	3.79	0.029	0.034
		RRMSE	1.05	1.06	1.03	2.35

4. Conclusions

In this work, we introduce a longitudinal simplified model of a DDWMR. In which the robot is assumed symmetrically, the left and the right motors/wheels are identical. The mass distributes equally to the left and the right. Based on this model, a sliding mode speed controller is designed and analyzed. The effects of the SMC parameters - the convergence and reaching rates, and simulation configuration - the time step, are evaluated. Considering the rising time, steady state error, and control ripple factors, the suitable values of the controller parameter and the simulation setting are selected.

The performance of the SMSC with optimized parameters is then investigated for the whole DDWMR system with two different time-step setting. The relative root mean square error (RRMSE) is defined and used as a metric to evaluate the velocity tracking performance of the left/right motors and the robot. Simulation results indicates that smaller time-step setting helps achieving better velocity tracking and smaller chattering amplitude. It is worth to notice that smaller time-step setting will cause a higher time computational consumption for simulation and stronger hardware capability for experimental system. Hence, suitable time-step setting should be taken into account when designing and implementing sliding mode control techniques.

References

[1] Maher, N., Elsheikh, G.A., Ouda, A.N., Anis, W.R., & Emara, T. (2022). Design and Implementation of a Wireless Medical Robot for Communication Within Hazardous Environments. *Wireless Pers Commun*, *122*, 1391—-1412.

[2] Yildirim, S. & Savas, S. (2021). Design of a Mobile Robot to Work in Hospitals and Trajectory Planning Using Proposed Neural Networks Predictors. *International Conference on Reliable Systems Engineering (ICoRSE)*, *305*, 32–45.

[3] Marchuk, V., Harmash, O., & Ovdiienko, O. (2020). World trends in warehousing logistics. *Intell Logist Supply Chain Manag*, *2*, 32–50.

[4] Barros, R., Silva Filho, J., Neto, J., & Nascimento, T. (2020). An open-design warehouse mobile robot. *In Proceedings of the 2020 Latin American Robotics Symposium (LARS), Brazilian Symposium on Robotics (SBR) and Workshop on Robotics in Education (WRE), Natal, Brazil*, 1–6.

[5] Azadeh, K., De Koster, R., & Roy, D. (2019). Robotized and automated warehouse systems: Review and recent developments. *Transp Sci*, *53*, 917–945.

[6] Hajduk, M. & Koukolová, L. (2015). Trends in industrial and service robot application. *Appl Mech Mater*, *791*, 161–165.

[7] Belanche, D., Casaló, L., Flavián, C., & Schepers, J. (2020). Service robot implementation: A theoretical framework and research agenda. *Serv Ind J*, *40*, 203—-225.

[8] Ma, T.T., Do, T.N., Pham, N.K., & Chau, N.K. (2016). Control of Pioneer P3-DX Robot through voice with mfcc featuring and Naive Bayes nearest neighbour algorithm. *1015625/vap2015000152*.

[9] SoftBank Robotics, For better business just add Pepper. *https://ussoftbankroboticscom/pepper*.

[10] You-bot store, KUKA YouBot Kinematics, Dynamics And 3D Model. *http://wwwyoubot-storecom/developers/kuka-youbot-kinematics-dynamics-and-3d-model*.

[11] Vu, T., Tran, A.M., Nguyen, B., & Tran, H. (2023). Development of Decentralized Speed Controllers for a Differential Drive Wheel Mobile Robot. *J Adv Eng Comput*, *7*, 76–94.

[12] Bayoumi, E.H.E. & Soliman, H. (2007). PID/PI tuning for minimal overshoot of permanent-magnet brushless DC motor drive using particle swarm optimization. *Electromotion*, *14*, 198–208.

[13] Kanojiya, R. & Meshram, P. (2012). Optimal tuning of PI controller for speed control of DC motor drive using particle swarm optimization. *2012 International Conference on Advances in Power Conversion and Energy Technologies (APCET)*, 1–6.

[14] Payakkawan, P., Klomkarn, K., & Sooraksa, P. (2009). Dual-line PID controller based on PSO for speed control of DC motors. *9th International Symposium on Communications and Information Technology ISCIT*, 134–139.

[15] Bansal, U.K. & Narvey, R. (2013). Speed Control of DC Motor Using Fuzzy PID Controller. *Adv Electron Electr Eng*, *3*, 1209–1220.

[16] Tran, A. & Vu, T. (2023). A study on general state model of differential drive wheeled mobile robots. *J Adv Eng Comput*, *7*, 174–186.

[17] Kim, S.K. & Ahn, C.K. (2021). DC Motor Speed Regulator via Active Damping Injection and Angular Acceleration Estimation Techniques. *IEEE/CAA Journal of Automatica Sinica*, *8*, 641–647.

[18] Kushwah, M. & Patra, P.A. (2014). Tuning PID Controller for Speed Control of DC Motor Using Soft Computing Techniques-A Review. *Adv Electron Electr Eng*, *4*, 141–148.

[19] Tir, Z., Oued, E., & Oued, E. (2017). Implementation of a Fuzzy Logic Speed Controller For a Permanent Magnet DC Motor Using a Low-Cost Arduino Platform. *The 5th International Conference on Electrical Engineering*, 29–32.

[20] Fukao, T., Nakagawa, H., & Adachi, N. (2000). Adaptive tracking control of a nonholonomic mobile robot. *IEEE Trans Robot Autom*, *16*, 609–615.

[21] Kim, M.S., Shin, J.H., & Lee, J.J. (2000). Design of a robust adaptive controller for a mobile robot. *Proc IEEE/RSJ Int Conf Intelligent Robots and Systems*, *3*, 1816—-1821.

[22] Das, T. & Kar., I. (2006). Design and Implementation of an Adaptive Fuzzy Logic-Based Controller for Wheeled Mobile Robots. *IEEE Transactions on Control Systems Technology*, *14*, 501—-510.

[23] Dongbing, G. & Huosheng, H. (2006). Receding horizon tracking control of wheeled mobile robots. *IEEE Trans Control Syst Technol*, *14*, 743—-749.

[24] Chen, H., Miao-Miao Ma, H., Wang, Z.Y., & Cai, Z.X. (2009). Moving horizon H infinity tracking control of wheeled mobile robots with actuator saturation. *IEEE Trans Control Syst Technol*, *21*, 449—-457.

[25] Pitanga, J., Araújo, H., Conceição, A., & Oliveira, G. (2015). Stable model-based predictive control for wheeled mobile robots using linear matrix inequalities. *Int Fed Autom Control*, *48*, 033—-038.

[26] Utkin, V.I., Gulder, J., & Shi, J. (1999). *Sliding Mode Control in Electromechanical Systems*. London, U.K.: Taylor & Francis.

[27] Alfonso, D., Gatto, G., Ignazio, M., & Alessandro, P. (2004). Second-order sliding-mode control of DC drives. *IEEE Transactions on Industrial Electronics*, *51*, 364–373.

[28] Amer, A.F., Sallam, E.A., & Sultan, I.A. (2016). Adaptive sliding-mode dynamic controller for nonholonomic mobile robots. *12th International Computer Engineering Conference*, 230–235.

[29] Vo, H., Tran, D., Thieu, T., Le, A., Dong, C., & Brandstetter, P. (2021). Sliding mode pwm direct torque controlled induction motor drive with kalman filtration of estimated load. *J Adv Eng Comput*, *5*, 265–276.

[30] Vo, H. (2023). Sliding Mode Speed Controller Design for Field Oriented Controlled PMSM Drive of an Electric Vehicle. *J Adv Eng Comput*, *7*, 164—-173.

[31] Nguyen, T., Nguyen, T., Le, K., Tran, H., & Jeon, J. (2023). An Adaptive Backstepping Sliding-Mode Control for Improving Position Tracking of a PermanentMagnet Synchronous Motor with a Nonlinear

Disturbance Observer. *IEEE Access*, *11*, 19173—19185.

[32] Ma, Y., Li, D., Li, Y., & Yang, L. (1992). Novel Discrete Compound Integral Terminal Sliding Mode Control with Disturbance Compensation for PMSM Speed System. *IEEE/ASME Transactions on Mechatronics*, *27*, 549—560.

[33] Huynh-Van, V. & Tran-Thanh, P. (2019). Discrete Sliding Mode Control Design for Piezoelectric Actuator. *J Adv Eng Comput*, *3*, 492—-502.

[34] Shi, J., Fu, F., Wang, Y., & Wang, J. (2016). SMC-based mobile robot stability control considering both matched and mismatched disturbances regulation and chatter alleviation. *2nd International Conference on Control, Automation and Robotics (ICCAR)*, 95–102.

[35] Keighobadi, J., Shahidi, M., Khajeh, A., & Fazeli, K. (2013). Dynamic Based SMC of Nonholonomic Mobile Robots. Positioning. *Positioning*, *4*, 153–159.

[36] X., H., Zheng, J.C., Chai, R., & Nguyen, T.H. (2021). Robust tracking control of a differential drive wheeled mobile robot using fast nonsingular terminal sliding mode. *Computers & Electrical Engineering*, *96*, 107488.

[37] Yigit, S. & Sezgin, A. (2023).). Trajectory Tracking via Backstepping Controller with PID or SMC for Mobile Robots. *Sakarya University Journal of Science*, *27*, 120–134.

About Authors

Tri-Vien VU received the B.Eng. degree in mechatronics from Hanoi University of Science and Technology, Ha noi, Viet nam, in 2005, and the M.Sc. and Ph.D. degrees from Da-yeh University, Changhua, Taiwan in 2011 and 2015, respectively. He works as a Lecturer at the Faculty Electrical and Electronics Engineering, Ton Duc Thang University, Ho Chi Minh City, Vietnam since 2015. His research interests include vehicle dynamic, mobile robot, power electronics, electrical drives.

Anh-Minh Duc TRAN received his B.S. and M.S. degrees in Control and Automation Engineering from Ho Chi Minh City University of Transport in 2008 and 2013, respectively, and his Ph.D. from Pukyong National University in Busan, Korea, in 2017. He is currently a lecturer at the Faculty of Electrical and Electronics Engineering, Ton Duc Thang University, Ho Chi Minh City, Vietnam. His research interests include system dynamics, robust, and nonlinear control.